Deletion of Gas2l3 in mice leads to specific defects in cardiomyocyte cytokinesis during development

Sabine Stopp[a], Marco Gründl[a], Marc Fackler[a], Jonas Malkmus[a], Marina Leone[b], Ronald Naumann[c], Stefan Frantz[d], Elmar Wolf[a,e], Björn von Eyss[a,1], Felix B. Engel[b], and Stefan Gaubatz[a,e,2]

[a]Theodor Boveri Institute, Biocenter, University of Wuerzburg, 97074 Wuerzburg, Germany; [b]Experimental Renal and Cardiovascular Research, Institute of Pathology, Department of Nephropathology, Friedrich-Alexander-Universität Erlangen-Nürnberg, 91054 Erlangen, Germany; [c]Transgenic Core Facility, Max-Planck-Institute of Molecular Cell Biology and Genetics, 01307 Dresden, Germany; [d]Department of Internal Medicine I, University Hospital Würzburg, 97080 Wuerzburg, Germany; and [e]Comprehensive Cancer Center Mainfranken, University of Wuerzburg, 97080 Wuerzburg, Germany

Edited by Helen M. Blau, Stanford University, Stanford, CA, and approved June 5, 2017 (received for review February 28, 2017)

GAS2L3 is a recently identified cytoskeleton-associated protein that interacts with actin filaments and tubulin. The in vivo function of GAS2L3 in mammals remains unknown. Here, we show that mice deficient in GAS2L3 die shortly after birth because of heart failure. Mammalian cardiomyocytes lose the ability to proliferate shortly after birth, and further increase in cardiac mass is achieved by hypertrophy. The proliferation arrest of cardiomyocytes is accompanied by binucleation through incomplete cytokinesis. We observed that GAS2L3 deficiency leads to inhibition of cardiomyocyte proliferation and to cardiomyocyte hypertrophy during embryonic development. Cardiomyocyte-specific deletion of GAS2L3 confirmed that the phenotype results from the loss of GAS2L3 in cardiomyocytes. Cardiomyocytes from *Gas2l3*-deficient mice exhibit increased expression of a p53-transcriptional program including the cell cycle inhibitor p21. Furthermore, loss of GAS2L3 results in premature binucleation of cardiomyocytes accompanied by unresolved midbody structures. Together these results suggest that GAS2L3 plays a specific role in cardiomyocyte cytokinesis and proliferation during heart development.

binucleation | cardiomyocytes | cytokinesis | GAS2L3

During embryogenesis and fetal life, the heart grows by rapid mitotic divisions of cardiomyocytes, producing hyperplastic growth. In the perinatal period, cell division ceases, cardiomyocytes withdraw from the cell cycle, and the further increase in cardiac mass is achieved through increase in cell size (hypertrophy) (1–3). The switch from hyperplastic to hypertrophic growth is characterized by extensive binucleation of cardiomyocytes. Cardiomyocyte binucleation is a consequence of a DNA synthesis followed by mitosis without cytokinesis. Thus, the cell division of postnatal cardiomyocytes is incomplete and karyokinesis is uncoupled from cytokinesis. In mice, binucleation starts around postnatal day (P)3 and by day 10, 85–90% of cardiomyocytes are binucleated (2). The physiological role of cardiomyocyte binucleation remains largely unknown, although it has been suggested that the increased number of mRNA transcripts from the two nuclei is necessary to maintain the metabolic function of hypertrophic cardiomyocytes (4, 5).

The processes that lead to proliferation arrest and binucleation of cardiomyocytes are also still poorly understood. Cell cycle regulators, growth factors, miRNAs, and nongenetic mechanisms have been implicated in formation of binucleated cells and cell cycle withdrawal of cardiomyocytes. For example, cardiomyocyte cell cycle arrest and binucleation is correlated with a down-regulation of positive regulators of the cell cycle such as cyclins and CDKs and up-regulation of cyclin-dependent kinase inhibitors such as p21 and p27 (6). A role for cyclins in cardiomyocyte cell cycle arrest is demonstrated by the finding that cyclin A overexpression delays cardiomyocyte cell-cycle withdrawal and promotes cardiac regeneration after myocardial infarction through the promotion of cytokinesis of adult cardiomyocytes (7, 8). Similarly, deletion of the homeobox protein Meis1 enhances proliferation of postnatal cardiomyocytes because it regulates the expression of cell cycle inhibitors such as $p16^{INK4A}$ and $p21^{CIP1}$ (9). Other pathways that have been implicated in the transition from proliferation to cell cycle exit include the Hippo pathway and neuregulin-1/ERBB2 signaling as well as the E2F–pocket-protein pathway and certain miRNAs (10–14).

In addition, nongenetic mechanisms have also been proposed to prevent cytokinesis of differentiated cardiomyocytes. During division of fetal cardiomyocytes, myofibrills have to disassemble. This disassembly occurs in two steps with Z-disk and actin filaments being disassembled first, followed by disassembly of the M-band and myosin filaments. It has been suggested that the highly ordered sarcomere structure of differentiated cardiomyocytes prevents this myofibrilar disassembly and, thus, presents a barrier to cytokinesis (4, 15, 16). In addition, the failure to assemble a contractile ring contributes to cardiomyocyte binucleation, and the cardiomyocyte cell cycle arrest is associated with centrosome disassembly (17, 18).

We and others have recently identified a role for GAS2L3 in cytokinesis and cytokinetic abscission (19–21). GAS2L3 belongs to the GAS2 family of four related proteins consisting of GAS2 and GAS2-like 1–3 (GAS2L1, GAS2L2, and GAS2L3). Previous studies linked the function of GAS2-proteins to cross-linking of actin and microtubule filaments in interphase and in growth-arrested cells (22–27). Unlike the other GAS2 family members, GAS2L3 is specifically expressed in mitosis and localizes to the mitotic spindle in metaphase, the midbody during cytokinesis, and the constriction zone during abscission (19, 20). RNA interference

Significance

Here, we demonstrate that mice lacking GAS2L3, a cytoskeleton-associated protein that interacts with actin filaments and tubulin, develop cardiomyopathy and heart failure after birth. During embryogenesis, cardiomyocytes rapidly divide. In the perinatal and neonatal period, cardiomyocytes withdraw from the cell cycle, binucleate, and the further increase in cardiac mass is achieved by hypertrophy. Germ-line deletion of *Gas2l3* results in decreased cardiomyocyte proliferation and in cardiomyocyte hypertrophy. Embryonal cardiomyocytes from *Gas2l3*-deficient mice exhibit increased expression of the cell cycle inhibitor p21 and display premature binucleation of cardiomyocytes due to defects in cytokinetic abscission. Together these results suggest that GAS2L3 plays a central role in cardiomyocyte proliferation and cytokinesis during development.

Author contributions: F.B.E. and S.G. designed research; S.S., M.G., M.F., J.M., M.L., R.N., and S.G. performed research; R.N., S.F., E.W., B.v.E., and F.B.E. contributed new reagents/analytic tools; S.S., M.G., S.F., F.B.E., and S.G. analyzed data; and S.G. wrote the paper.

The authors declare no conflict of interest.

This article is a PNAS Direct Submission.

Data deposition: The data reported in this paper have been deposited in the Gene Expression Omnibus (GEO) database, https://www.ncbi.nlm.nih.gov/geo (accession no. GSE91078).

[1]Present address: Leibniz Institute on Aging, Fritz Lipmann Institute e.V., 07745 Jena, Germany.

[2]To whom correspondence should be addressed. Email: stefan.gaubatz@biozentrum.uni-wuerzburg.de.

This article contains supporting information online at www.pnas.org/lookup/suppl/doi:10.1073/pnas.1703406114/-/DCSupplemental.

(RNAi)-mediated depletion of GAS2L3 and overexpression studies have implicated GAS2L3 in cytokinesis, chromosome segregation, and abscission.

The in vivo function of GAS2L3 in mammals remains unknown. Here, we show that mice with a germ-line deletion of *Gas2l3* die postnatally from dilated cardiomyopathy. Further studies implicate GAS2L3 in cardiomyocyte proliferation and cytokinesis during embryonic development.

Results

GAS2L3 Is Required for Postnatal Viability. To investigate the in vivo function of mammalian GAS2L3, we generated a knockout mouse model in which exon 6 of *Gas2l3* is flanked by loxP sites (Fig. S1 *A*–*C*). Exon 6 encodes for part of the N-terminal–conserved CH domain that is involved in binding of GAS2L3 to actin. Deletion of exon 6 results in a frame-shift and, thus, no functional GAS2L3 protein can be produced when exon 6 is deleted. Loss of *Gas2l3* expression was verified by crossing animals with the targeted allele of *Gas2l3* with a mouse line ubiquitously expressing a $CreER^{T2}$ transgene, which can be activated by 4-hydroxytamoxifen (4-OHT). Upon treatment of mouse embryonic fibroblasts isolated from $Gas2l3^{fl/fl}$;$CreER^{T2}$ mice with 4-OHT, exon 6 was successfully deleted and *Gas2l3* mRNA and protein expression was eliminated (Fig. S1 *D*–*F*). To investigate the role of GAS2L3 during embryonic development, we converted the conditional allele into a nonconditional knockout ($^{-/-}$) allele by crossing $Gas2l3^{fl/fl}$ mice with Zp3-Cre mice, expressing Cre-recombinase in the female germ line (28) (Fig. S1*A*).

$Gas2l3^{+/-}$ mice were intercrossed, and offspring was genotyped (Fig. S2*A*). $Gas2l3^{-/-}$ pups were recovered at the expected Mendelian frequency (Fig. S2*B*). However, at weaning (3 wk), only 7 of 113 mice (6%) were homozygous for the *Gas2l3* knockout, significantly below the expected frequency of 25% ($P < 0.01$), indicating a role for GAS2L3 in the early postnatal period (Fig. S2 *B* and *C*). A few mice survived into adulthood, but they all either died before the age of 4 mo or were euthanized because they became moribund. Heterozygous $Gas2l3^{+/-}$ mice were found at normal frequency and showed no phenotype.

Loss of Gas2l3 Results in Dilated Cardiomyopathy with Fibrosis. Further characterization revealed severe cardiac enlargement in homozygous $Gas2l3^{-/-}$ animals, whereas no gross abnormalities in other organs were observed (Fig. 1*A* and Fig. S3). The heart to body weight of 14-d-old $Gas2l3^{-/-}$ mice was significantly increased compared with age-matched wild-type or heterozygous control animals (Fig. 1*B*). Histological analysis of $Gas2l3^{-/-}$ hearts revealed ventricular chamber dilation as manifested by a reduction in wall thickness and enlargement (Fig. 1 *C* and *D*). In approximately 30% of $Gas2l3^{-/-}$ mice, intracardiac thrombi that were attached tightly to the ventricular wall were present. Thrombus formation likely contributes to the death of some of the $Gas2l3^{-/-}$ animals. Transthoracic echocardiography of 6-wk-old mice confirmed dilated cardiomyopathy with a reduction in left ventricular posterior wall thickness and increased ventricular diameter (Fig. 1 *E* and *F*). Changes in cardiac dimensions were accompanied by decreased contractility and markedly impaired cardiac function as evidenced by a strongly reduced fractional shortening (FS) compared with wild-type mice (Fig. 1*F*).

Further characterization by immunofluorescence staining for cardiac troponin T (cTnT) revealed a disordered organization of cardiomyocytes in $Gas2l3^{-/-}$ hearts (Fig. 2*A*). Quantification of cell size by wheat germ agglutinin (WGA) staining showed that cell sizes in the heart of $Gas2l3^{-/-}$ mice at P7 and P14 (Fig. 2*B*) were strongly increased. At later stages, a significant interstitial

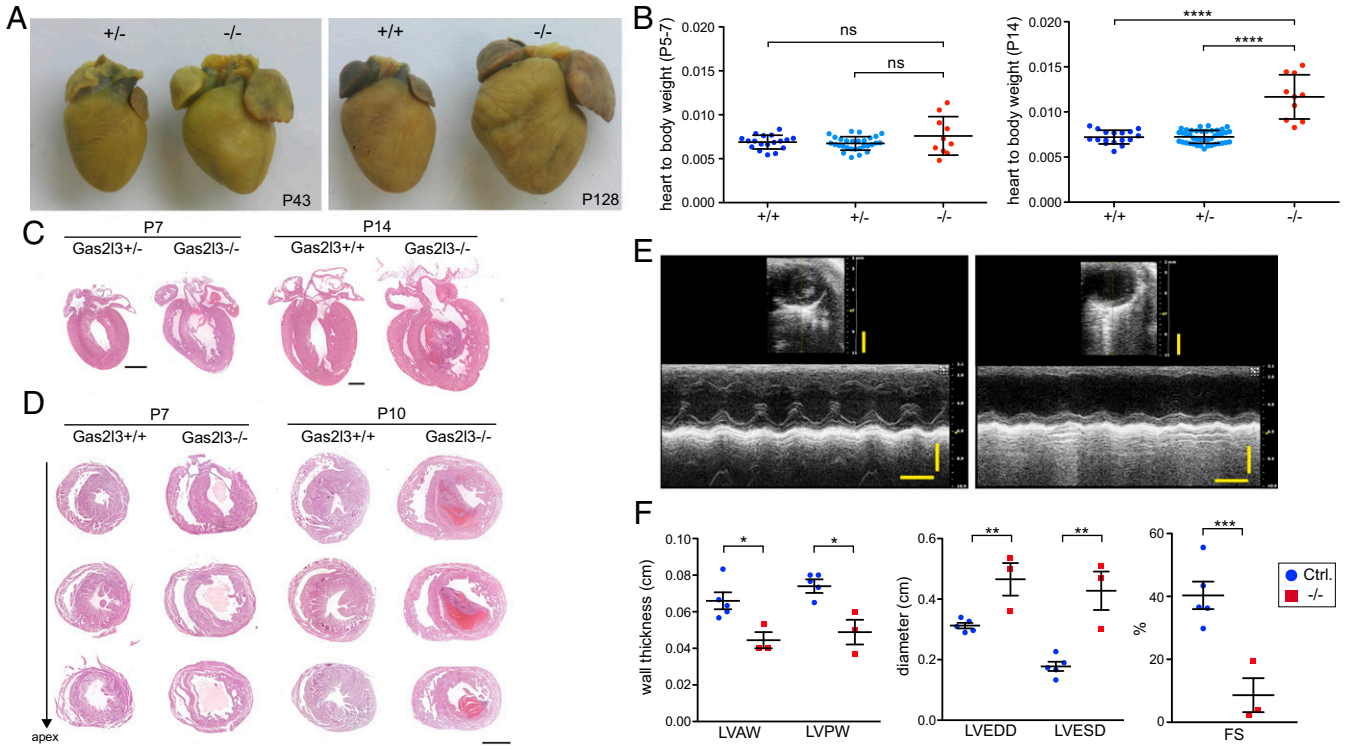

Fig. 1. Postnatal lethality and dilated hearts of *Gas2l3* knockout mice. (*A*) Fixed hearts from 43-d and 128-d-old animals. Wild-type ($^{+/+}$) and heterozygote ($^{+/-}$) mice served as controls. (*B*) Heart-to-body weight of 5- to 7-d-old and 14-d-old $Gas2l3^{-/-}$ and control mice. $n > 10$ mice per group. (*C*) H&E-stained sagittal sections demonstrating dilated ventricles in $Gas2l3^{-/-}$ animals compared with control mice. (*D*) H&E stained transverse sections of $Gas2l3^{-/-}$ and $Gas2l3^{+/+}$ hearts. (*E* and *F*) Cardiac function was analyzed by echocardiography in 6-wk-old mice. (*E*) Representative images of echocardiographic analysis. (*F*) Quantification of LVAW and LVPW (left ventricular anterior and posterior wall thickness), LVEDD and LVESD left (ventricular end-diastolic and end-systolic dimensions) and fractional shortening (FS). $n =$ 3–5 mice per group. (Scale bars: *C*, 0.5 mm; *D*, 1 mm; *E*, vertical 2 mm, horizontal 0.1 s.) $^{*}P < 0.05$; $^{**}P < 0.01$; $^{***}P < 0.001$; $^{****}P < 0.0001$; ns, not significant.

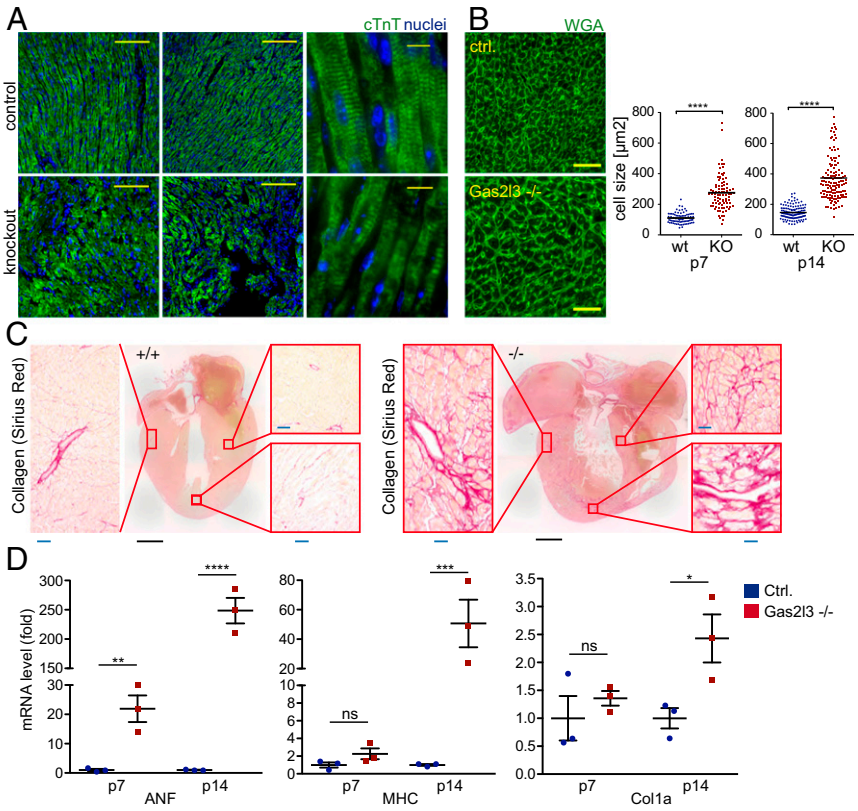

Fig. 2. Hypertrophy and fibrosis of Gas2l3 knockout hearts. (*A*) Immunofluorescence staining of cTNT in a wild-type and *Gas2l3*$^{-/-}$ heart at P5 (green). Nuclei were stained with Hoechst (blue). (*B*) WGA staining at P7 and P14. A quantification of the cross-sectional area is shown on the right. (*C*) Sirius red staining demonstrating fibrosis in *Gas2l3*$^{-/-}$ hearts. (*D*) mRNA expression of the indicated genes was analyzed by RT-qPCR in P7 and P14 hearts. Expression was normalized to 18S rRNA. $n = 3$ mice per group. (Scale bars: *A, Left* and *Center*, 75 µm; *A, Right*, 10 µm; *B*, 50 µm; *C*, 500 µm.) *$P < 0.05$; **$P < 0.01$; ***$P < 0.001$; ****$P < 0.0001$; ns, not significant.

fibrosis developed in *Gas2l3*$^{-/-}$ hearts, as evidenced by Sirius Red staining for myocardial collagen (Fig. 2*C*). Consistent with these observations, mRNA levels of the fibrosis marker collagen 1a were increased at P14 in *Gas2l3* knockout hearts. Expression levels of the hypertrophy markers atrial natriuretic peptide (ANF) and β-myosin heavy chain (MHC) were also increased, and ANF was already elevated in *Gas2l3*$^{-/-}$ hearts at P7 (Fig. 2*D*).

To determine whether the phenotype is due to loss of GAS2L3 in cardiomyocytes or whether it is an indirect consequence of loss of GAS2L3 in other cell types such as cardiac fibroblasts, conditional *Gas2l3* mice were crossed to mice that express Cre-recombinase from the cardiac-specific Nkx2.5 promoter (Fig. S4*A*) (29). The heart-to-body weight of *Nkx2.5-Cre;Gas2l3*$^{fl/fl}$ mice was significantly increased compared with control mice (Fig. S4*B*). Histological staining revealed a cardiac phenotype with enlarged and dilated hearts and with interstitial fibrosis (Fig. S4 *C* and *D*). Together these results indicate that the *Gas2l3* k.o. phenotype is due to a cardiomyocyte-intrinsic defect.

GAS2L3 Is Dispensable in the Adult Heart. To test whether GAS2L3 is required in the postnatal heart, we deleted *Gas2l3* in neonatal *Gas2l3*$^{fl/fl}$;*CreER*^{T2} mice by tamoxifen injection to activate the CreER^{T2} recombinase (Fig. S5*A*). PCR genotyping verified recombination of *Gas2l3* in the heart (Fig. S5*B*). The heart weight to body weight after deletion of *Gas2l3* was unchanged, and no chamber dilation or fibrosis was observed after deletion of *Gas2l3* (Fig. S5 *C* and *D*), indicating that neonatal deletion of *Gas2l3* does not result in dilated cardiomyopathy. The lack of a phenotype in postnatal mice confirms a specific requirement for GAS2L3 during embryonic development.

To determine whether the expression pattern of *Gas2l3* is consistent with its exclusive role during embryonic development, we performed real-time quantitative PCR (RT-qPCR) with RNA isolated from cardiac tissue at different embryonic and postnatal stages. This analysis demonstrated that *Gas2l3* expression was highest during early embryonic stages and significantly decreased at neonatal stages (Fig. S5*E*).

Reduced Cardiomyocyte Proliferation and Induction of p53 > p21 in Gas2l3 Knockout Mice. Cardiomyocytes undergo two distinct growth phases during development with hyperplastic growth during midgestation and hypertrophic growth characterized by binucleation during the perinatal period (2). Quantification of total cardiomyocyte number per heart by enzymatic disaggregation and cell counting showed that at embryonic day 14.5 (E14.5), the cardiomyocyte number was slightly reduced in *Gas2l3*$^{-/-}$ mice compared with control mice (Fig. 3*A*). In control animals, the cardiomyocyte number per heart increased more than 10-fold between E14.5 and P7. In contrast, cardiomyocytes numbers increased less than twofold in *Gas2l3*$^{-/-}$ mice during the same time period. Consequently, at P7, cardiomyocyte cell numbers were markedly reduced in *Gas2l3*$^{-/-}$ mice compared with control mice. Cardiomyocyte size was comparable in *Gas2l3* knockout mice and control mice at E14.5 (Fig. 3*B*). However, at E18.5 and at all later timepoints, cardiomyocytes from *Gas2l3*$^{-/-}$ mice were significantly hypertrophic compared with control cardiomyocytes, consistent with WGA staining of histological sections (Fig. 3*B*).

To establish how the loss of GAS2L3 results in reduced cellularity, we next analyzed the cell cycle marker Ki67 by immunofluorescence staining. Cardiomyocytes were identified by staining for cardiac troponin T. The proportion of Ki67-positive cardiomyocytes was significantly decreased in *Gas2l3*$^{-/-}$ hearts compared with littermate controls (Fig. 3*C*), indicating a role for GAS2L3 in cardiomyocyte proliferation. Importantly, the proliferation of embryonic hepatocytes was not affected by the loss of *Gas2l3* (Fig. S6*A*). The reduced cardiomyocyte proliferation probably accounts for the decrease in cardiomyocyte numbers.

To further investigate the pathways resulting in growth arrest of *Gas2l3*$^{-/-}$ cardiomyocytes, we performed RNA sequencing (RNAseq) on E18.5 hearts. Gene ontology analysis of genes with decreased expression in *Gas2l3*$^{-/-}$ hearts are linked to processes related to cell cycle regulation, mitosis, and chromosome segregation, consistent with the phenotype of *Gas2l3* deletion (Fig. 4*A* and S7*A*). Furthermore, gene set enrichment analysis (GSEA) revealed an increased expression of genes known to be activated

DEVELOPMENTAL BIOLOGY

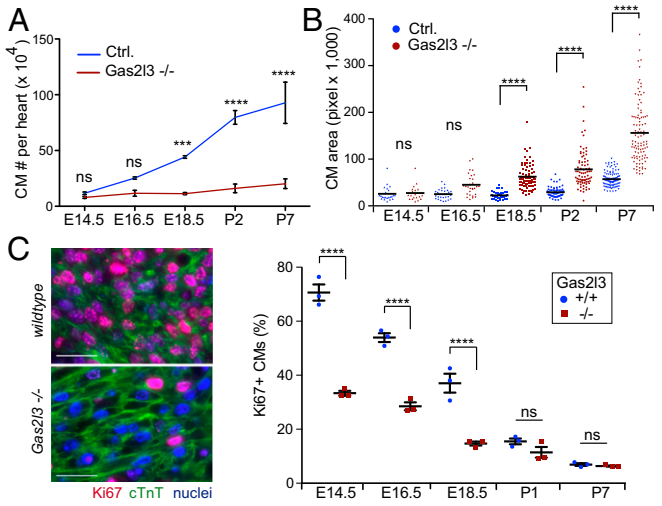

Fig. 3. Decreased proliferation of *Gas2l3* knockout cardiomyocytes. (*A*) Total number of cardiomyocytes in hearts from control mice and *Gas2l3*$^{-/-}$ mice at the indicated developmental time points. Cardiomyocytes were isolated, fixed, and quantified with a hematocytometer. (*B*) Area of fixed cardiomyocytes at the indicated time points. (*C, Left*) Representative immunofluorescence staining of Ki67 and cTnT in a E14.5 heart section. (Scale bars: 25 μm.) (*Right*) Quantification of Ki67-positive cardiomyocytes in E14.5, E16.5, E18.5, P1, and P7 hearts. ***$P < 0.001$; ****$P < 0.0001$; ns, not significant.

by the p53 tumor suppressor in *Gas2l3* k.o. hearts, including the CDK inhibitor p21 (Cdkn1a) (Fig. 4 *B* and *C*). p21 acts as a CDK inhibitor to indirectly inhibit phosphorylation of the retinoblastoma (pRB) proteins by CDKs. It is normally not expressed in embryonal cardiomyocytes and induced in adult cardiomyocytes (30). Increased expression of p21 and additional p53-target genes in embryonic *Gas2l3*$^{-/-}$ hearts was verified by qPCR (Fig. 4*D*). Consistent with the transcriptional up-regulation of p21, induction of p53 and p21 in *Gas2l3*$^{-/-}$ hearts was detected by immunoblotting (Fig. 4*E*). Furthermore, pRB hypophosphorylation was increased in *Gas2l3*$^{-/-}$ hearts compared with control hearts, suggesting that induction of p21 contributes to the cell cycle arrest of *Gas2l3*-deficient cardiomyocytes by activating pRB. Although a subset of the p53-dependent genes up-regulated in *Gas2l3*$^{-/-}$ hearts has been associated with apoptosis, *Gas2l3* deletion did not result in an increase in apoptosis as determined by immunoblotting of heart lysates for cleaved caspase 3 or by TUNEL assays of histological sections at E18.5 or P14 (Fig. S7 *B* and *C*).

Premature Binucleation and Defective Cytokinesis in Gas2l3-Deficient Cardiomyocytes. Given that cardiomyocytes undergo binucleation during the perinatal period contributing to the cell cycle arrest, we next determined the fraction of mononucleated and binucleated cardiomyocytes at different developmental stages. At E14.5, binucleation of *Gas2l3*$^{-/-}$ cardiomyocytes was low and comparable to that of control cardiomyocytes (Fig. 5 *A* and *B*). In contrast, at later time points, significant differences in binucleation were detected. At E16.5, E18.5, and P2, 30–60% of *Gas2l3*$^{-/-}$ cardiomyoctes were binucleated, whereas only a small fraction of control cardiomyocytes were binucleated, as expected. At P7, 60% *Gas2l3*$^{-/-}$ were binucleated compared with 90% binucleation in control mice. Taken together, *Gas2l3*$^{-/-}$ cardiomyocyte binucleate significantly earlier during cardiac development than wild-type cardiomyocytes. However, in the absence of GAS2L3, a significant proportion of cardiomyocytes are mononucleated at P7, suggesting that during development, a proportion of mononucleated *Gas2l3*$^{-/-}$ cardiomyocytes withdraw prematurely from the cell cycle, contributing to the reduced total number of cardiomyocytes per heart. A role for GAS2L3 in mitosis and cytokinesis is also indicated by the reduced number of cells staining positive for phosphorylated (Ser10) histone H3, a marker of mitotic cells, and the reduced number of cardiomyocytes undergoing cytokinesis at E14.5 (Aurora B-positive) (Fig. 5 *C* and *D*). In contrast to cardiomyocytes, no difference in hepatocyte binucleation was observed in *Gas2l3*$^{-/-}$ mice compared with wild-type littermates (Fig. S6*B*).

The increased binucleation of *Gas2l3*$^{-/-}$ cardiomyocytes could be an indirect effect of the decreased number in cardiomyocytes and the consequently increased hemodynamic load that usually occurs only after birth and has been linked to cardiomyocyte binucleation (5). To address whether binucleation is a secondary, noncell autonomous consequence of *Gas2l3* deletion, we performed experiments with cultured cardiomyocytes. Cardiomyocytes were isolated from embryos expressing a conditional, "floxed" allele of Gas2l3 (*Gas2l3*$^{fl/fl}$) and a CreER^{T2} transgene with a 4-OHT–inducible Cre recombinase. Recombination of *Gas2l3* by addition of 4-OHT was verified by PCR genotyping (Fig. S8*A*). Before recombination, the majority of cardiomyocytes were mononucleated, as expected (Fig. 5 *E* and *G*). After deletion of *Gas2l3*, approximately 22% of cardiomyocytes became binucleated. Thus, the binucleation phenotype is not an indirect effect of increased hemodynamic stress. Rather these data suggest an intrinsic role for GAS2L3 in division of cardiomyocytes. Importantly, control cardiomyocytes of the *Gas2l3*$^{+/+}$; *CreER*^{T2} genotype-treated 4-OHT were mononucleated, as expected, indicating that the increase in binucleated cells is not an off-target effect of Cre-recombinase (Fig. S8 *B* and *C*).

Further characterization of the defect in mitosis by immunofluorescence analysis showed that loss of GAS2L3 had no obvious effect on localization of Anillin, Aurora B, and Myosin II to the central spindle and the midbody during telophase and cytokinesis (Fig. S9 *A* and *B*). Importantly, however, cells with unresolved cytokinetic midbody structures were significantly increased upon deletion of Gas2l3, indicating failed abscission (Fig. 5 *F* and *G*). The subcellular localization of GAS2L3 in cardiomyocytes to the central spindle and to the midbody region during telophase and cytokinesis, as determined by confocal microscopy with an antiserum raised

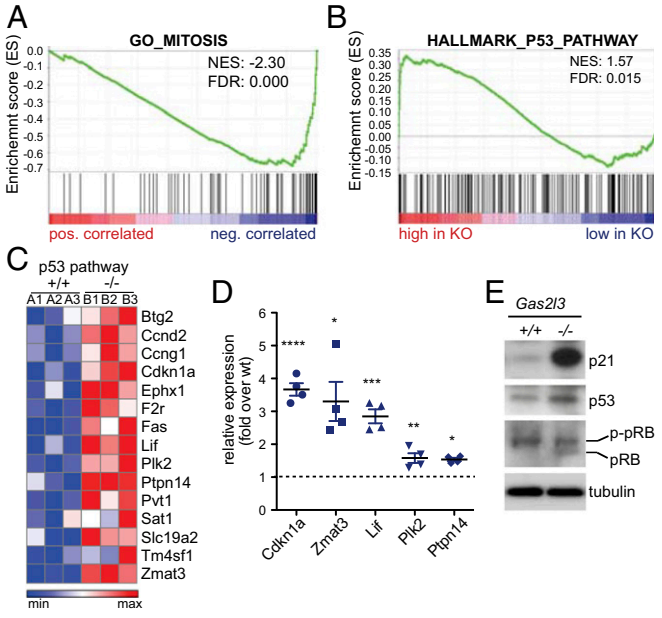

Fig. 4. RNA-Seq analysis of *Gas2l3*$^{-/-}$ hearts. (*A*) RNA-Seq was performed on RNA isolated from E18.5 wild-type and Gas2l3$^{-/-}$ hearts ($n = 3$ hearts per group). GSEA plot for the GO term mitosis. (*B*) GSEA identified a significant enrichment of targets of the p53 transcription factor in *Gas2l3* knockout hearts. (*C*) Heatmaps of the p53 target genes enriched in *Gas2l3*$^{-/-}$ hearts compared with wild-type hearts. (*D*) RT-qPCR was used to confirm up-regulation of the indicated p53-target genes. (*E*) The levels of p21, p53, and hypophosphorylated pRB in lysates from wild-type ($^{+/+}$) and *Gas2l3*$^{-/-}$ hearts at E18.5 were determined by immunoblotting. Tubulin served as a loading control. *$P < 0.05$;**$P < 0.01$; ***$P < 0.001$; ****$P < 0.0001$.

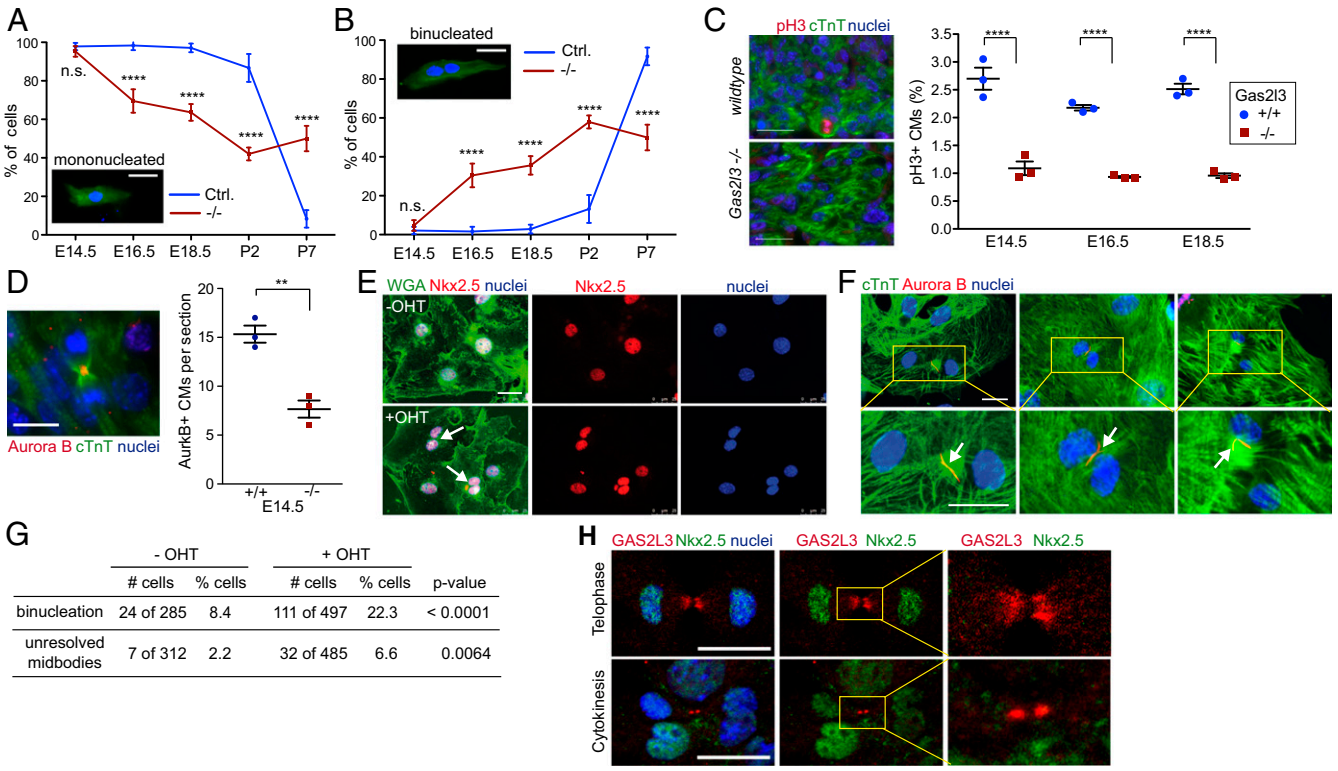

G

	- OHT		+ OHT		
	# cells	% cells	# cells	% cells	p-value
binucleation	24 of 285	8.4	111 of 497	22.3	< 0.0001
unresolved midbodies	7 of 312	2.2	32 of 485	6.6	0.0064

Fig. 5. Defective cytokinesis in *Gas2l3*-deficient cardiomyocytes. (*A* and *B*) Quantification of mononucleated and binucleated cardiomyocytes in control and *Gas2l3*$^{-/-}$ mice. (*Inset*) Example immunofluorescence images of mononucleated and binucleated cardiomyocytes stained with Connexin 43 and Hoechst are shown. (*C*) Representative immunofluorescence staining of phospho-histone H3 (Ser10) (pH3) and cTnT in an E14.5 heart section (*Left*). Quantification of pH3-positive cardiomyocytes in E14.5, E16.5, and E18.5 heart sections. (*D*) Representative confocal immunofluorescence image of Aurora B and cTnT in an E16.5 heart section (*Left*). Quantification of Aurora B-positive cardiomyocytes per section (*Right*). (*E*) E14.5 *Gas2l3*$^{fl/fl}$;*CreER*^{T2} were treated for 96 h with 4-OHT and stained for WGA (green), Nkx2.5 (red), and Hoechst. Arrows point to binucleated cells. (*F*) Detection of unresolved midbody structures in *Gas2l3*$^{fl/fl}$;*CreER*^{T2} cardiomyocytes by staining for Aurora B (red). Cardiomyocytes were identified by staining for cTnT (green). Nuclei were stained with Hoechst. (*G*) Quantification of binuclear E14.5 *Gas2l3*$^{fl/fl}$;*CreER*^{T2} cardiomyocytes and cardiomyocytes with unresolved midbodies after treatment with or without 4-OHT for the indicated times. (*H*) Localization of GAS2L3 to the spindle midzone and the midbody of cardiomyocytes as detected by staining with an antiserum directed at murine GAS2L3 (red). Cardiomyocytes were identified by staining for Nkx2.5 (green). (Scale bars: *A* and *B*, *Insets*, *C*, *Left*, *E*, and *F*, 25 μm; *D*, *Left*, 75 μm; *H*, 5 μm.) $^{**}P < 0.01$; $^{****}P < 0.0001$; ns, not significant.

against murine GAS2L3, is consistent with its participation in cytokinetic abscission in cardiomyocytes (Fig. 5*H*).

Discussion

Until now, the in vivo role of GAS2L3 in mammals was unknown. We show here that GAS2L3 plays a key role in cardiomyocyte proliferation and cytokinesis during heart development in mice. During late embryonic development, loss of GAS2L3 leads to a drastically reduced number of cardiomyocytes and to premature cardiomyocyte binucleation. Cardiomyocyte loss in *Gas2l3*-deficient mice is compensated for by a strong increase in cardiomyocyte size. This compensatory hypertrophy, however, is not sufficient to maintain organ function after birth and is associated with interstitial fibrosis, ventricular dilatation, and contractile dysfunction resulting in early death of the animals.

GAS2L3 is required for cardiomyocyte mitosis during a relative narrow window during embryonic development, and it is dispensable for the adult cardiomyocytes that have exited from the cell cycle. It has been observed that loss of general cell cycle regulators, e.g., cyclin E or *N*-myc in mice, results in defects in embryonic cardiomyocyte proliferation and prenatal lethality (31–33). In contrast, *Gas2l3*$^{-/-}$ animals survive until a few weeks after birth, indicating a requirement for GAS2L3 relatively late in cardiac development. This observation suggests that GAS2L3 is dispensable for cytokinesis of early, immature embryonic cardiomyocytes. During differentiation from embryonic to a postnatal stage, the complexity of the sarcomere structure of cardiomyocytes gradually increases (34). It is known that highly organized myofibrils create an obstacle to cytokinesis and that sarcomeric structures have to disassemble before cell division can occur (17, 35). The failure of more advanced embryonic *Gas2l3*$^{-/-}$ cardiomyocyte to divide suggests a possible role for GAS2L3 in coordinating cytokinesis of cardiomyocytes with the breakdown of highly organized sarcomeric structures, whereas cytokinesis of less differentiated earlier cardiomyocytes may be independent of GAS2L3. This model could also explain why the phenotype of *Gas2l3* deletion is specific to the heart and why other organs are not affected by the loss of GAS2L3. Alternatively, the lack of a phenotype in other organs could be due to compensation by other members of the GAS2 family.

Down-regulation of *Gas2l3* expression correlates with the time point when binucleation and cell cycle withdrawal of cardiomyocytes takes place. We note that the developmental expression profile of *Gas2l3* in the heart is similar to other proteins involved in cytokinesis that are expressed at high levels before birth and down-regulated postnatally when cardiomyocyte binucleate and exit from the cell cycle (36). Mitosis-specific expression of Gas2l3 is driven by the Myb–MuvB (MMB) complex (19), an evolutionary conserved multiprotein complex that either associates with the p130 pocket protein and with E2F4 to form DREAM to represses transcription or with B-MYB to activate transcription (37–39). MMB is a master regulator of genes with functions in mitosis and cytokinesis, suggesting that it could be involved in regulation of a larger set of cytokinesis genes involved in heart development. Further experiments are necessary to address this possibility.

Materials and Methods

Mice. Detailed information on generation of *Gas2l3*$^{-/-}$ and conditional *Gas2l3*^{fl} mice and on genotyping of mice can be found in *SI Materials and Methods*. All animal experiments were carried out according to protocols that were approved by an institutional committee (Tierschutzkommission der Regierung von Unterfranken).

Cardiomyocyte Isolation and Cultivation. Primary cardiomyocytes were isolated from E14.5 embryos by enzymatic digestion by using a cardiomyocyte isolation kit (Pierce). Cardiomyocytes were cultured on fibronectin-coated dishes in DMEM with 10% heat-inactivated FBS at 37 °C and 5% CO_2. To induce the deletion of *Gas2l3*, conditional cardiomyocytes were treated with 100 nM 4-OHT (Sigma).

Determination of Cardiomyocyte Numbers and Nucleation. Isolation of cardiomyocytes was essentially performed as described (9). In brief, fresh hearts were harvested and fixed in 4% PFA for 2 h. Next, hearts were incubated with a mixture of collagenase D (2.4 mg/mL, Roche) and collagenase B (1.8 mg/mL, Roche) for 12 h at 37 °C with slow shaking. Cardiomyocytes were stained with Connexin 43 antibodies. DNA was counterstained with Hoechst 33548. Cardiomyocyte cell numbers were determined by using a Neubauer chamber.

RNA-Seq Analysis. RNA-Seq is described in *SI Materials and Methods*. The data have been deposited in National Center for Biotechnology Information's (NCBI's) Gene Expression Omnibus (GEO) (40) and are accessible through GEO Series accession no. GSE91078 (https://www.ncbi.nlm.nih.gov/geo/query/acc.cgi?acc=GSE91078).

Statistical Analysis. Statistical analyses were performed by using Prism 5 (GraphPad). Statistical significance was determined by using Student's *t* test (two groups), one-way ANOVA with Bonferroni posttest (>2 groups) or Fisher's exact test (nominal data). $P < 0.05$ was considered statistically significant. $^{*}P < 0.05$;$^{**}P < 0.01$; $^{***}P < 0.001$; $^{****}P < 0.0001$.

Additional methods and a list of antibodies are provided in *SI Materials and Methods*.

ACKNOWLEDGMENTS. We thank Laura Kowalski for help with immunohistochemistry, Sandra Umbenhauer and Susi Spahr for excellent technical help; Manfred Gessler, Christine Field, Michaela Kuhn, Elisabeth Ehler, and Eva Geissinger for reagents, advice, and helpful discussions; and all members of the laboratory for suggestions and critical reading of the manuscript. This work was funded by Deutsche Forschungsgemeinschaft Grants DFG GA575/5-2 and GA575/9-1 (to S.G.), ELAN Program Grant 12-11-05-1-Engel, and the Emerging Fields Initiative Cell Cycle in Disease and Regeneration (CYDER) by the Friedrich-Alexander-Universität Erlangen-Nürnberg (to F.B.E.).

1. Li F, Wang X, Capasso JM, Gerdes AM (1996) Rapid transition of cardiac myocytes from hyperplasia to hypertrophy during postnatal development. *J Mol Cell Cardiol* 28: 1737–1746.
2. Soonpaa MH, Kim KK, Pajak L, Franklin M, Field LJ (1996) Cardiomyocyte DNA synthesis and binucleation during murine development. *Am J Physiol* 271:H2183–H2189.
3. van Amerongen MJ, Engel FB (2008) Features of cardiomyocyte proliferation and its potential for cardiac regeneration. *J Cell Mol Med* 12:2233–2244.
4. Ahuja P, Sdek P, MacLellan WR (2007) Cardiac myocyte cell cycle control in development, disease, and regeneration. *Physiol Rev* 87:521–544.
5. Zebrowski DC, Engel FB (2013) The cardiomyocyte cell cycle in hypertrophy, tissue homeostasis, and regeneration. *Rev Physiol Biochem Pharmacol* 165:67–96.
6. Paradis AN, Gay MS, Zhang L (2014) Binucleation of cardiomyocytes: The transition from a proliferative to a terminally differentiated state. *Drug Discov Today* 19: 602–609.
7. Chaudhry HW, et al. (2004) Cyclin A2 mediates cardiomyocyte mitosis in the postmitotic myocardium. *J Biol Chem* 279:35858–35866.
8. Shapiro SD, et al. (2014) Cyclin A2 induces cardiac regeneration after myocardial infarction through cytokinesis of adult cardiomyocytes. *Sci Transl Med* 6:224ra27.
9. Mahmoud AI, et al. (2013) Meis1 regulates postnatal cardiomyocyte cell cycle arrest. *Nature* 497:249–253.
10. D'Uva G, et al. (2015) ERBB2 triggers mammalian heart regeneration by promoting cardiomyocyte dedifferentiation and proliferation. *Nat Cell Biol* 17:627–638.
11. Heallen T, et al. (2011) Hippo pathway inhibits Wnt signaling to restrain cardiomyocyte proliferation and heart size. *Science* 332:458–461.
12. Piccoli M-T, Gupta SK, Thum T (2015) Noncoding RNAs as regulators of cardiomyocyte proliferation and death. *J Mol Cell Cardiol* 89:59–67.
13. Sdek P, et al. (2011) Rb and p130 control cell cycle gene silencing to maintain the postmitotic phenotype in cardiac myocytes. *J Cell Biol* 194:407–423.
14. Wadugu B, Kühn B (2012) The role of neuregulin/ErbB2/ErbB4 signaling in the heart with special focus on effects on cardiomyocyte proliferation. *Am J Physiol Heart Circ Physiol* 302:H2139–H2147.
15. Li F, Wang X, Gerdes AM (1997) Formation of binucleated cardiac myocytes in rat heart: II. Cytoskeletal organisation. *J Mol Cell Cardiol* 29:1553–1565.
16. Li F, Wang X, Bunger PC, Gerdes AM (1997) Formation of binucleated cardiac myocytes in rat heart: I. Role of actin-myosin contractile ring. *J Mol Cell Cardiol* 29: 1541–1551.
17. Engel FB, Schebesta M, Keating MT (2006) Anillin localization defect in cardiomyocyte binucleation. *J Mol Cell Cardiol* 41:601–612.
18. Zebrowski DC, et al. (2015) Developmental alterations in centrosome integrity contribute to the post-mitotic state of mammalian cardiomyocytes. *eLife* 4:4.
19. Wolter P, et al. (2012) GAS2L3, a target gene of the DREAM complex, is required for proper cytokinesis and genomic stability. *J Cell Sci* 125:2393–2406.
20. Pe'er T, et al. (2013) Gas2l3, a novel constriction site-associated protein whose regulation is mediated by the APC/C Cdh1 complex. *PLoS One* 8:e57532.
21. Fackler M, Wolter P, Gaubatz S (2014) The GAR domain of GAS2L3 mediates binding to the chromosomal passenger complex and is required for localization of GAS2L3 to the constriction zone during abscission. *FEBS J* 281:2123–2135.
22. Stroud MJ, Kammerer RA, Ballestrem C (2011) Characterization of G2L3 (GAS2-like 3), a new microtubule- and actin-binding protein related to spectraplakins. *J Biol Chem* 286:24987–24995.
23. Stroud MJ, et al. (2014) GAS2-like proteins mediate communication between microtubules and actin through interactions with end-binding proteins. *J Cell Sci* 127: 2672–2682.
24. Brancolini C, Bottega S, Schneider C (1992) Gas2, a growth arrest-specific protein, is a component of the microfilament network system. *J Cell Biol* 117:1251–1261.
25. Goriounov D, Leung CL, Liem RKH (2003) Protein products of human Gas2-related genes on chromosomes 17 and 22 (hGAR17 and hGAR22) associate with both microfilaments and microtubules. *J Cell Sci* 116:1045–1058.
26. Zucman-Rossi J, Legoix P, Thomas G (1996) Identification of new members of the Gas2 and Ras families in the 22q12 chromosome region. *Genomics* 38:247–254.
27. Zhang T, Dayanandan B, Rouiller I, Lawrence EJ, Mandato CA (2011) Growth-arrest-specific protein 2 inhibits cell division in Xenopus embryos. *PLoS ONE* 6:e24698.
28. de Vries WN, et al. (2000) Expression of Cre recombinase in mouse oocytes: A means to study maternal effect genes. *Genesis* 26:110–112.
29. Stanley EG, et al. (2002) Efficient Cre-mediated deletion in cardiac progenitor cells conferred by a 3'UTR-ires-Cre allele of the homeobox gene Nkx2-5. *Int J Dev Biol* 46: 431–439.
30. Poolman RA, Gilchrist R, Brooks G (1998) Cell cycle profiles and expressions of p21CIP1 AND P27KIP1 during myocyte development. *Int J Cardiol* 67:133–142.
31. Geng Y, et al. (2003) Cyclin E ablation in the mouse. *Cell* 114:431–443.
32. Moens CB, Auerbach AB, Conlon RA, Joyner AL, Rossant J (1992) A targeted mutation reveals a role for N-myc in branching morphogenesis in the embryonic mouse lung. *Genes Dev* 6:691–704.
33. Charron J, et al. (1992) Embryonic lethality in mice homozygous for a targeted disruption of the N-myc gene. *Genes Dev* 6:2248–2257.
34. Hirschy A, Schatzmann F, Ehler E, Perriard J-C (2006) Establishment of cardiac cytoarchitecture in the developing mouse heart. *Dev Biol* 289:430–441.
35. Ahuja P, Perriard E, Perriard J-C, Ehler E (2004) Sequential myofibrillar breakdown accompanies mitotic division of mammalian cardiomyocytes. *J Cell Sci* 117:3295–3306.
36. Ahuja P, et al. (2007) Re-expression of proteins involved in cytokinesis during cardiac hypertrophy. *Exp Cell Res* 313:1270–1283.
37. Sadasivam S, Duan S, DeCaprio JA (2012) The MuvB complex sequentially recruits B-Myb and FoxM1 to promote mitotic gene expression. *Genes Dev* 26:474–489.
38. Schmit F, et al. (2007) LINC, a human complex that is related to pRB-containing complexes in invertebrates regulates the expression of G2/M genes. *Cell Cycle* 6:1903–1913.
39. Osterloh L, et al. (2007) The human synMuv-like protein LIN-9 is required for transcription of G2/M genes and for entry into mitosis. *EMBO J* 26:144–157.
40. Edgar R, Domrachev M, Lash AE (2002) Gene Expression Omnibus: NCBI gene expression and hybridization array data repository. *Nucleic Acids Res* 30:207–210.
41. Poueymirou WT, et al. (2007) F0 generation mice fully derived from gene-targeted embryonic stem cells allowing immediate phenotypic analyses. *Nat Biotechnol* 25: 91–99.
42. Farley FW, Soriano P, Steffen LS, Dymecki SM (2000) Widespread recombinase expression using FLPeR (flipper) mice. *Genesis* 28:106–110.
43. Hameyer D, et al. (2007) Toxicity of ligand-dependent Cre recombinases and generation of a conditional Cre deleter mouse allowing mosaic recombination in peripheral tissues. *Physiol Genomics* 31:32–41.
44. Subramanian A, et al. (2005) Gene set enrichment analysis: A knowledge-based approach for interpreting genome-wide expression profiles. *Proc Natl Acad Sci USA* 102: 15545–15550.
45. Frantz S, et al. (2004) Peroxisome proliferator activated-receptor agonism and left ventricular remodeling in mice with chronic myocardial infarction. *Br J Pharmacol* 141:9–14.